WILEY ✧ ION

Design and implementation of a real-time software receiver for BDS-3 signals

Yang Gao [ID] | Zheng Yao [ID] | Mingquan Lu

Department of Electronic Engineering, Tsinghua University, Beijing, China

Correspondence
Zheng Yao, Department of Electronic Engineering, Tsinghua University, Beijing, China.
Email: yaozheng@tsinghua.edu.cn

Abstract

The BeiDou Navigation Satellite System (BDS) is currently building its third phase (BDS-3), which will provide services to users around the world. In addition to backward compatibility with BDS-2, BDS-3 satellites are equipped with the B1C and B2 interoperable signals for compatibility with GPS and Galileo systems. To evaluate performance and optimize processing methods, we designed and implemented a real-time software receiver with the ability to process all BDS-3 signals in parallel. A complete description of all signal processing aspects is given. To reduce the reliance on high-performance hardware while maintaining the independent analysis capabilities of acquisition performance in real-time software receivers, a B1I-aided acquisition method for reducing the search space of other signals from the same satellite is applied. An unambiguous tracking method is proposed to solve the ambiguity problem of the Quadrature Multiplexed Binary Offset Carrier (QMBOC) signal that can be used for matching reception of the pilot component of the B1C signal.

1 | INTRODUCTION

As part of the evolution of the third phase of the BeiDou Navigation Satellite System (BDS-3), 18 Medium Earth Orbit (MEO) satellites and one Geostationary Earth Orbit (GEO) satellite have been placed on orbit as of 9 December 2018.[1] In 2020, the full constellation of BDS-3 satellites will be fully deployed. BDS-3 with full operational capability will provide Positioning, Navigation, and Timing (PNT) services to worldwide users and help improve PNT precision for global receivers. It is China's contribution to the world in the domain of GNSS.[2,3] BDS-3 satellites transmit a variety of signals at different frequencies as allocated by the International Telecommunication Union (ITU). In addition to backward compatibility with conventional B1I and B3I signals, BDS-3 satellites are equipped with the B1C and B2 interoperable signals for compatibility with GPS and Galileo systems. The traditional B2I signal will be gradually replaced by the B2b signal with the construction of the global BDS.[4-7]

In order to evaluate the actual performance of new BDS-3 signals and optimize their processing methods, receivers capable of processing all civil BDS-3 signals should be developed according to the published BDS Interface Control Documents (ICDs).[4-7] Compared with hardware receivers, software-defined receivers are more efficient to develop, more flexible to configure, and more suitable to use in the construction phase of the new GNSS.[8] Therefore, developing a software receiver that can process all civil BDS-3 signals was a good choice in recent years.

According to the computing capability of the receiver, the existing software-defined receiver architectures can generally be divided into two categories. The first category of architectures is collectively referred to as post-processing software receivers, since in this category the intermediate frequency (IF) signals are first recorded and then processed offline, meaning that these receivers cannot be used in applications that have high demands on real-time processing abilities. In contrast, the second

category of architectures, which is collectively referred to as real-time software receivers, requires that the IF signals be processed at a speed no less than the speed at which they were acquired, thus placing high demands on the computing capability of the receiver. With the development of graphics processing unit (GPU) parallel computing, especially the emergence of the Compute Unified Device Architecture (CUDA) parallel programming model, GPU-based software receivers have been rapidly developed, and more and more real-time software receivers with GPU-based architecture are emerging.[9-11]

Compared with post-processing software receivers, a real-time software receiver is more suitable for signal quality monitoring and signal performance evaluation. However, to the author's knowledge, there is currently no existing real-time software receiver with the ability to process all BDS-3 signals in parallel. Therefore, we use the GPU-based architecture to design and implement a real-time software receiver capable of processing all civil BDS-3 signals. In addition, a complete description of all signal processing aspects including front-end processing and baseband signal processing is given. The work and contribution of our discussion mainly include three aspects.

First, a GPU-based real-time software receiver architecture is designed and implemented that can process all civil BDS-3 signals in parallel. It could be used in signal performance analysis, signal quality monitoring, and processing algorithms development. In addition, most receiver parameters can be flexibly configured, which means the performance comparison under different parameters can be easily conducted. Therefore, the proposed real-time software receiver architecture could provide guidance to receiver designers who need to analyze and process BDS-3 signals.

Second, a B1I aided acquisition method is applied to reduce the search space of other BDS-3 signals from the same satellite. Compared with traditional acquisition methods, the B1I aided acquisition method utilizes the highly correlated characteristics between the B1I signal and other signals from the same satellite to achieve faster acquisition and to reduce the reliance on high-performance hardware. Therefore, the applied B1I aided acquisition method can provide reference value for the acquisition of multiple signals at different frequencies in other GNSSs.

Third, an unambiguous tracking method based on multidimensional loops estimation is proposed to solve the ambiguity problem of the Quadrature Multiplexed Binary Offset Carrier signal (QMBOC), which can be used for matching reception of the pilot component of the B1C signal. The actual test results verify the correctness of the proposed method.

The remainder of the paper is organized as follows. We first review the civil signal plan of BDS-3. Then, we explain the GPU-based real-time software receiver architecture. The proposed B1I aided acquisition method and unambiguous tracking algorithm of QMBOC signal are illustrated in detail in the subsequent two sections. A set of test results is then provided in a special section to verify the validity of the receiver architecture and proposed algorithms. Finally, conclusions and future work are discussed.

2 | BDS-3 SIGNALS REVIEW

As the last phase of the construction and development of BDS, BDS-3 will provide PNT services to users around the world. Like other GNSSs, BDS-3 satellites broadcast multiple signals at different frequencies to meet demands from different applications.

Table 1 shows the BDS-3 signal plan. In addition to backward compatibility with conventional B1I and B3I signals, BDS-3 satellites introduce B1C and B2 interoperable signals to achieve compatibility with GPS and Galileo systems.

In order to interoperate with GPS L5 and Galileo E5 signals, BDS-3 satellites broadcast wideband signals at two frequencies in the B2 band with center frequencies at 1176.45 and 1207.14 MHz, respectively.[6] Both B2a and B2b signals are composed of pilot and data components that are in phase-quadrature with each other. Their spreading codes (rate is 10.23 MHz) are multiplexed into a constant envelope signal before transmitting in order to reduce the satellite payload and multiplexing loss. The asymmetric constant envelope binary offset carrier (ACE-BOC) modulation and multiplexing technique with its low-complexity implementation from Yao, Zhang, and Lu[12] is adopted to provide a flexible power configuration when multiplexing the B2 components. ACE-BOC, which marries multicarrier spread-spectrum modulation with constant envelope multiplexing, can combine two signals consisting of data and pilot components at arbitrary power ratio onto two sidebands of a split-spectrum composite signal. Therefore, the composite signal can either be received as two sets of Quadrature Phase-Shift Keying (QPSK) signals located at two different center frequencies, respectively, or as a wideband signal.

The current ICD only describes the structure of the B2a signal, which is presented as a QPSK(10) modulated signal.[6] The baseband complex envelope of the B2a signal is

$$s_{B2a}(t) = s_{B2a\_data}(t) + j s_{B2a\_pilot}(t), \quad (1)$$

where

TABLE 1 BDS-3 signal plan

Signal	Component	left Frequency/MHz	Modulation	Phase/°	Pseudorandom Code Rate/Mcps	Pseudorandom Code Period	Subcarrier/MHz	Baseband Signal Sampling Rate/MHz	Remarks
B2a	Pilot	1176.45	BPSK (10)	90	10.23	1 ms	--	20	New signal
	Data		BPSK (10)	0	10.23	1 ms	--		
B2b	Pilot	1207.14	BPSK (10)	90	10.23	1 ms	--	20	New signal
	Data		BPSK (10)	0	10.23	1 ms	--		
B3I	--	1268.52	BPSK (10)	0	10.23	1 ms	--	20	Backward compatible
B1I	--	1561.098	BPSK (2)	0	2.046	1 ms	--	5	Backward compatible
B1C	Pilot	1575.42	QMBOC	90/0	1.023	10 ms	1.023/6.138	5/20	New signal
	Data		BOC (1,1)	0	1.023	10 ms	1.023		

Abbreviation: BDS-3, BeiDou Navigation Satellite System.

$$s_{\text{B2a\_data}}(t) = \frac{1}{\sqrt{2}} D_{\text{B2a\_data}}(t) \cdot C_{\text{B2a\_data}}(t), \tag{2}$$

$$s_{\text{B2a\_pilot}}(t) = \frac{1}{\sqrt{2}} C_{\text{B2a\_pilot}}(t), \tag{3}$$

where $D_{\text{B2a\_data}}(t)$ is the navigation message, $C_{\text{B2a\_data}}(t)$ and $C_{\text{B2a\_pilot}}(t)$ are the ranging code for the data and pilot channel, respectively. Both $s_{\text{B2a\_data}}(t)$ and $s_{\text{B2a\_pilot}}(t)$ are modulated in Binary Phase-Shift Keying (BPSK) mode. The power ratio between the data component and the pilot component is 1:1.

In order to interoperate with GPS L1C and Galileo E1 signals, BDS-3 satellites broadcast the B1C signal with center frequency at 1575.42 MHz.[5] The B1C signal is composed of pilot and data components that are both based on BOC modulation. The data component adopts BOC(1,1) modulation. In order to meet the multiplexed MBOC spectral constraint,[13] the pilot component adopts QMBOC modulation and multiplexing technique by placing the narrowband BOC(1,1) component and the wideband BOC(6,1) component in phase quadrature.[14] Like other MBOC modulated signals, the QMBOC signal can either be received in mismatched processing mode with low complexity by ignoring the wideband BOC(6,1) component or in matching reception mode by considering all components.[15]

The baseband complex envelope of the B1C signal is

$$s_{B1C}(t) = \underbrace{\frac{1}{2} D_{B1C\_data}(t) \cdot C_{B1C\_data}(t) \cdot \text{sign}(\sin(2\pi f_{sc\_B1C\_a} t))}_{s_{B1C\_data}(t)},$$
$$+ \underbrace{\sqrt{\frac{1}{11}} C_{B1C\_pilot}(t) \cdot \text{sign}(\sin(2\pi f_{sc\_B1C\_b} t))}_{s_{B1C\_pilot\_b}(t)},$$
$$+ j\underbrace{\sqrt{\frac{29}{44}} C_{B1C\_pilot}(t) \cdot \text{sign}(\sin(2\pi f_{sc\_B1C\_a} t))}_{s_{B1C\_pilot\_a}(t)},$$

$$\tag{4}$$

where D_{B1C_data} is the navigation message; $C_{B1C\_data}(t)$ and $C_{B1C\_pilot}(t)$ are the ranging code for the data and pilot channel, respectively; $f_{sc\_B1C\_a} = 1f_0$ and $f_{sc\_B1C\_b} = 6f_0$ are the subcarrier frequency of the narrowband BOC(1,1) component and the wideband BOC(6,1) component, respectively; $f_0 = 1.023$ MHz is the GNSS baseline frequency; and sgn(x) is the sign function, which takes the value of 1 for $x \geq 0$ and -1 for $x < 0$. The power ratio between the data component and the pilot component is 1:3.

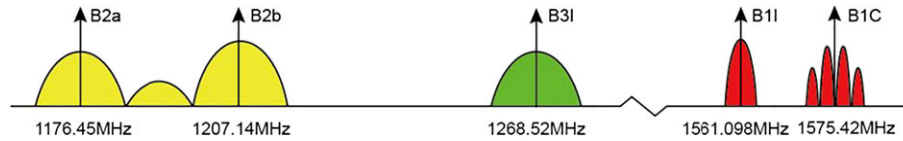Figure 1 presents the spectrum of civil BDS-3 signals. It can be seen from Figure 1 that there are multiple

FIGURE 1 The spectrum of civil BeiDou Navigation Satellite System (BDS-3) signals [Color figure can be viewed at wileyonlinelibrary. com and www.ion.org]

signals in both the B1 and B2 bands, which means they could be processed together in the front-end module. In addition, since these signals from the same satellite are based on the same reference clock, there are strong correlations in their phase relationships. Therefore, the joint processing of multiple BDS-3 signals could be of interest in the next few years.

3 | REAL-TIME SOFTWARE RECEIVER ARCHITECTURE

In order to evaluate the actual performance of new BDS-3 signals and optimize their processing methods, we designed and implemented a real-time software receiver with the ability to process all BDS-3 signals in parallel. Figure 2 shows the architecture of the real-time software receiver for BDS-3 signals. As can be seen from Figure 2, the real-time software receiver mainly consists of five modules, which are full L-band antenna with low-noise amplifier (LNA), down converter, data acquisition module, personal computer (PC) with central processing unit (CPU) and GPU, and storage and display module.

First, the full L-band antenna with LNA receives all radio frequency (RF) signals from visible satellites in the horizon. Second, the front-end down converts the received RF signals to the IF signals. Third, the data acquisition module converts the analog IF signals into digital baseband signals. Then all the baseband signal processing, which contains acquisition, tracking, message extraction, and positioning calculation, is completed by CPU and GPU in an ordinary PC. The outputs of the tracking module include navigation messages and observation results. The navigation messages including ephemeris are extracted by the message extraction module

according to the ICDs,[4-7] and the extraction results are passed to the positioning module. After receiving the observation results from the tracking module and the extracted navigation messages from the message extraction module, the single-point positioning solutions can be obtained by the positioning module. Finally, all the observation results, extracted navigation messages, and single-point positioning solutions are stored in the database and read by the display module.

It should be noted that the full L-band antenna with LNA is a mature commercial product that we can easily get. In addition, the single-point positioning solutions can be processed by open-source software,[16] and the display module could be realized by high-level programming language. Therefore, we mainly focus on the design and implementation of the front-end module, data acquisition module, and baseband signal processing module.

3.1 | Front-end and data acquisition module

Figure 3 shows the detailed data flow diagram from analog RF signals to digital baseband signals. First, all RF navigation signals from visible satellites in the horizon can be received by the full L-band antenna with LNA. Second, the received RF signals are divided into four analog channels to complete down conversion and IF filter processing by the front-end. The corresponding frequency range and signals are shown in Table 2. Third, the obtained analog IF signals are input into the A/D converters of the data acquisition module to get digital IF signals. Then, each channel of digital IF signals is sequentially processed by the corresponding digital down conversion (DDC), low-pass filter (LPF), and decimation
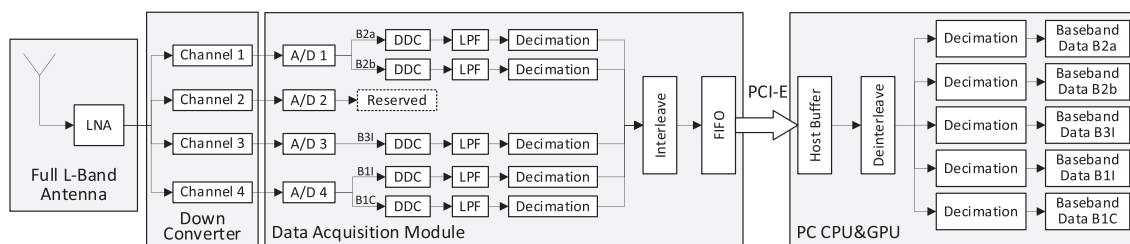

FIGURE 2 Block diagram of real-time software receiver for BeiDou Navigation Satellite System (BDS-3) signals
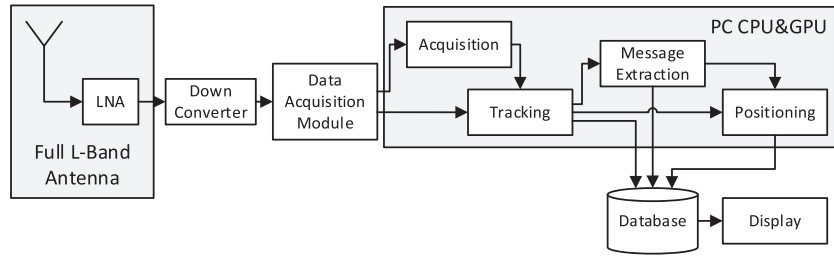
FIGURE 3 Data flow block diagram from analog radio frequency (RF) signals to digital baseband signals

TABLE 2 The frequency range of down converter

Channel	Frequency Range/MHz	Signals
1	1164-1215	B2a/B2b
2	1215-1260	Reserved
3	1260-1300	B3I
4	1559-1610	B1I/B1C

to obtain the zero-IF signals. Next, these digital baseband signals are interleaved and input into First In, First Out (FIFO) order. Finally, these FIFOs containing baseband signals are transmitted to the buffer of the host PC through high-speed serial interface Peripheral Component Interconnect Express (PCI-E). After a deinterleaving operation and proper decimation, all digital baseband signals of BDS-3 can be obtained and wait to be processed. The final sampling rates of baseband signals are shown in Table 1.

The down converter we chose is the BDC-L-210-4C developed by HeBei Doheart Electronic Technology Co., LTD. This front-end divides the whole L frequency band into four intervals, and each interval corresponds to an analog down-conversion channel. The output IF of all channels is 210 MHz, which is convenient for the unified processing of the signals in the data acquisition module.

The data acquisition module we chose is the X5-210 M developed by the Innovative Integration Company. This data acquisition card has four simultaneously sampled A/D channels that operate at rates up to 250 MHz (14-bit). Additionally, it has a powerful field-programmable gate array (FPGA) signal processing core to accomplish DDC, LPF, and decimation, and a high-performance PCI-E host interface. The sampling rate we chose at the A/D converter is 240 MHz, which is a high sampling rate to reduce the design difficulty of the analog IF filter in the front-end. In addition, 8-bit quantization is used to meet the needs for signal monitoring. After DDC and LPF operations, each IF signal is transferred into a zero-IF signal with in-phase and quadrature-phase components. After the first decimation in the data acquisition module and the second decimation in the PC, the sampling rate of each baseband

signal is transferred from 240 MHz to the corresponding sampling rate in Table 1.

There are two factors that mainly affect the processing performance of a real-time software receiver. One factor is the sampling rate of the baseband signal, which is no less than the width of the main lobe of the baseband signal. The higher the sampling rate, the higher the data-processing rate required. The other factor is the coherent integration time, which is no less than the pseudorandom code period of the baseband signal. A longer-coherent integration time requires that more baseband data must be processed. Therefore, it can be concluded that the matching reception of the pilot component of the B1C signal is the most complicated case in the reception processing of all civil BDS-3 signals because it has the highest sampling rate and the longest-coherent integration time.

3.2 | Baseband signal processing module

Figure 4 shows the generic architecture of the baseband signal processing in the PC, which consists of acquisition, tracking, message extraction, and positioning calculation. First, the acquisition module uses GPU to find coarse estimates for code phase and Doppler frequency of baseband signals in parallel. Then, these coarse values are used to initialize the tracking channels. Second, the tracking module uses GPU to continuously track the baseband signals and gets fine estimates of code phase, Doppler frequency, and carrier phase for each channel. Third, once a channel reaches the stable tracking state, the message extraction module demodulates the navigation message
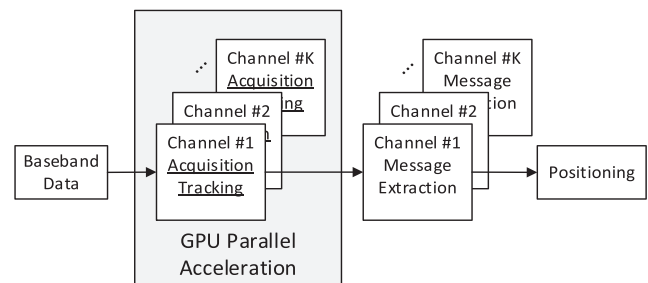

FIGURE 4 Baseband signal processing architecture

from the channel after bit synchronization and frame synchronization. Finally, the positioning module uses pseudorange and navigation message to calculate the single-point positioning solutions of the receiver.

It can be easily seen that the acquisition module and the tracking module are the most computationally intensive portions of the baseband signal processing phase. Since these computationally intensive operations are relatively simple and could be parallelized, GPU parallel computing is very well suited to handle these tasks and improve the processing performance of the real-time software receiver. The parallel programming model we chose is CUDA developed by NVIDIA, which has lots of libraries and templates to help us complete the parallel computing operations during the acquisition and tracking phases. The following sections will describe the implementation and optimization of the CUDA-based acquisition and tracking modules in detail.

4 | ACQUISITION

The acquisition of the baseband signal is a two-dimensional (2-D) search operation performed in the 2-D space constructed by Doppler frequency and code phase. Taking the B1I signal as an example, the received baseband signal after the front-end and data acquisition module can be modeled as follows:

$$r_{baseband}(t-\tau) = AC_{B1I}(t-\tau)\cos(2\pi f_D(t-\tau)+\varphi) + n(t), \quad (5)$$

where A is the signal amplitude, $C_{B1I}(t)$ is the ranging code, τ is the code delay, f_D is the Doppler frequency, φ is the carrier phase, and $n(t)$ is zero-mean Gaussian white noise. The main purpose of the acquisition module is to find the coarse estimates of code phase τ and Doppler frequency f_D.

4.1 | CUDA-based acquisition module

The acquisition, which is a 2-D search operation, is completed by performing correlation between the local replica signal and the received baseband signal. According to the implementation form of the correlation operation, the existing acquisition algorithms are mainly divided into three categories, namely, sequential search, parallel frequency search, and parallel code search.[17]

The conventional sequential search directly performs correlation operation in the time domain.[18] The correlation result between the local replica code and the received ranging code can be modeled as follows:

$$z(n) = \frac{1}{N}\sum_{m=0}^{N-1} x(m)y(m-n), \quad (6)$$

where N is the length of pseudorandom code, and $x(n)$ and $y(n)$ are the ranging code of local replica signal and received baseband signal, respectively. Since the time domain sequential search is a computationally intensive operation and cannot be parallelized, it is not advised to use sequential search in the whole 2-D search space in the design of real-time software receiver.

The parallel code search is the parallel search operation in the code dimension based on Fourier transformation.[19] By performing a Discrete Fourier Transform (DFT) on Equation 6, we obtain

$$Z(k) = \frac{1}{N}X(k)Y^*(k), \quad (7)$$

where $X(k)$, $Y(k)$, and $Z(k)$ are the DFT of $x(n)$, $y(n)$, and $z(n)$, respectively, and operator * is the conjugate operation. It can be seen from Equatiions 6 and 7 that the correlation integral result of two signals in the time domain is equal to the inverse DFT of the multiplication of their DFT results. Using Fast Fourier Transform (FFT) operations to accelerate the calculation of DFT,[20] Equation 6 can be represented as follows:

$$z(n) = \text{IFFT}\{\text{FFT}(x(n))\cdot\text{FFT}^*(y(n))\}. \quad (8)$$

Therefore, the parallel code search can greatly speed up the search operations in the ranging code dimension.

Similar to the parallel code search, the parallel frequency search is the parallel search operation in the frequency dimension based on Fourier transformation, which could save time required for frequency dimension search.

Compared with the conventional sequential search and parallel frequency search, the parallel code search could parallelize many more search operations in the 2-D search space. Therefore, the parallel code search algorithm is again very well suited for the acquisition phase of the software receiver. Figure 5 shows the parallel code search algorithm that we chose in the real-time software receiver.
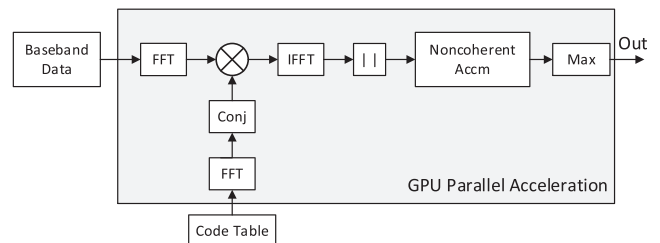

FIGURE 5 Parallel code search algorithm

The CUDA parallel programming platform could help us to efficiently complete the acquisition of the baseband signal. The code dimension search, which adopts the parallel code search algorithm based on FFT and IFFT operations, could be sped up by using the highly optimized and tested cuFFT library provided by CUDA. Since the received baseband signals are transferred from the time domain to the frequency domain due to the Fourier transformation, the Doppler frequency search could be optimized by the vector shift operation in the frequency dimension. In addition, since the noncoherent accumulation and maximum operations can be treated as tree-based reduction problems, these operations could be optimized by the parallel reduction based on the sequential addressing and loop unrolling in CUDA.[21]

4.2 | B1I-aided acquisition method

The acquisition of the baseband signals in a real-time software receiver could be completed by the CUDA-based parallel acceleration. However, the amount of data that needs to be temporarily stored and finally processed is proportional to the sampling rate, the number of channels, the coherent integration periods, and the times of noncoherent accumulation. Therefore, in order to reduce the amount of data required to be processed and reduce the dependence on high-performance hardware, the optimization algorithms in the acquisition phase of the real-time software receiver are of interest. An L1 C/A-aiding method to acquire the L2C signal was proposed in the study of Lim.[22] Combined acquisition methods for L1 C/A and L1C signals were proposed in previous studies.[23,24] These methods utilize the strong correlations between the signal with short ranging code and the signals with long ranging codes from the same satellite. Similar to these, a B1I-aided acquisition method for reducing the 2-D search space of other BDS-3 signals from the same satellite can be applied in our real-time software receiver.

Figure 6 shows the procedure of the B1I-aided acquisition method. First, the parallel code search algorithm is used to acquire the B1I signal whose ranging code length is the shortest among all civil BDS-3 signals. The coarse estimate of Doppler frequency $\widehat{f}_{DB1I}$ and code phase $\widehat{\tau}_{B1I}$ can be obtained. Second, these two estimates are used to calculate the 2-D search subspaces of other signals from the same satellite. Taking the frequency dimension of the 2-D search subspace into consideration first, it is not difficult to prove that the Doppler frequency of the received signal is proportional to the carrier center frequency ignoring the influence of the ionosphere. The relationship is as follows:
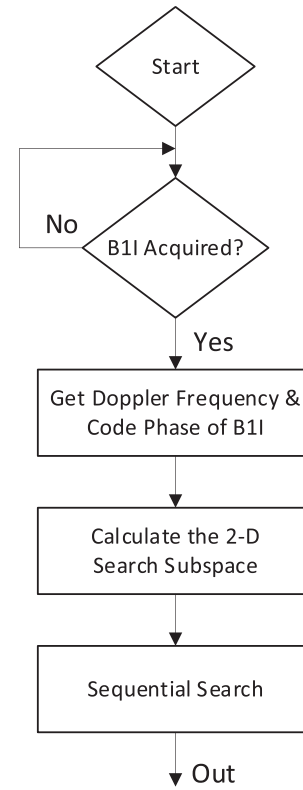

FIGURE 6 Procedure of B1I aided acquisition method

$$f_D = \frac{f_{RF} v_{dm}}{c}, \tag{9}$$

where f_{RF} is the carrier center frequency, v_{dm} is the relative speed between the satellite and receiver, and c is the speed of light. Therefore, the Doppler frequency of other signals from the same satellite should be within the range of the center $f_D = \frac{f_{RF}}{f_{B1I}} \widehat{f}_{DB1I}$ and length $\pm f_{bin\_B1I}$, where f_{B1I} is the carrier center frequency of the B1I signal, and f_{bin} is the frequency bin width in the frequency dimension, which should satisfy the relationship[25]:

$$f_{bin} \leq \frac{2}{3T_{coh}}, \tag{10}$$

where T_{coh} is the coherent integration time. Next, considering the code dimension of the 2-D search subspace, it should be noted that the resolution of the code dimension search is actually specified by the sampling rate instead of 1/2 chip width. Therefore, the code phase of other signals from the same satellite should be within the range of the center $\tau_{RF} = \frac{SF_{RF}}{SF_{B1I}} \widehat{\tau}_{B1I}$ and length $\pm \frac{2SF_{RF}}{SF_{B1I}}$, where SF is the sampling rate of the corresponding BDS-3 signals that can be obtained from Table 1. In addition, since the pseudorandom code period of the B1C signal is 10 times that of the B1I signal, it is also necessary to consider the integral multiple parts of the B1I code period when calculating the range of the B1C code phase. It is not difficult to

prove that the code phase of the B1C signal from the same satellite should be within the range of the center

$$\tau_{RF} = \frac{SF_{B1C}}{SF_{B1I}}\widehat{\tau}_{B1I} + \frac{\text{mod}(k, 10)}{1000}SF_{B1C} \text{ and length } \pm\frac{2SF_{RF}}{SF_{B1I}},$$

where $k = 1, 2, 3 ... , 10$ milliseconds is the integral multiple times of B1I code period, and $\text{mod}(x, y)$ is the modulo function, which takes the value of the remainder after division of x by y. Finally, after obtaining the 2-D search subspace, the time domain sequential search could be used to complete the acquisitions of other signlas from the same satellite.

5 | TRACKING

The tracking of the baseband signal is mainly completed using the correlation between the local replica signal and the received baseband signal, which can be expressed as follows:

$$\chi(\Delta\tau) = \frac{1}{T}\int_0^T r_{baseband}(t - \tau)\cdot\widehat{r}_{local}(t - \widehat{\tau})\mathrm{d}t, \qquad (11)$$

where $\chi(\Delta\tau)$ is the correlation result, $\widehat{r}_{local}(t - \widehat{\tau})$ is the local replica signal, $\widehat{\tau}$ is the estimate of code delay, and $\Delta\tau = \tau - \widehat{\tau}$ is the estimation error of the code delay. The main purpose of the tracking phase is to continuously track the received baseband signals and get fine estimates of code phase, Doppler frequency, and carrier phase for each channel.

5.1 | CUDA-based correlator

In the tracking phase of the conventional BPSK signals, receivers always generate three local code components, which are early (E) replica $C(t - \widehat{\tau} - \Delta_c/2)$, prompt (P) replica $C(t - \widehat{\tau})$, and late (L) replica $C(t - \widehat{\tau} + \Delta_c/2)$. Δ_c is the discriminator spacing between E and L replicas for the code loop, and it is assumed to be in the range $0 < \Delta_c \leq T_c$, where $T_c = 1/f_c$ is the pseudorandom code period. Figure 7 shows the tracking architecture of the real-time software receiver for conventional BPSK signals. The largest computing workload in the tracking phase is from the correlation between the local replica signal and the received baseband signal, which mainly consists of two operations: multiplication and accumulation. Since these two computationally intensive operations could be parallelized, it is quite reasonable to use the CUDA parallel programming model for the correlation.

In order to strive for peak performance of GPU, the CUDA-based correlator can be optimized in two ways: algorithmic optimizations and code optimizations. An efficient way to implement the algorithmic optimization of the correlator is to first multiply and then immediately
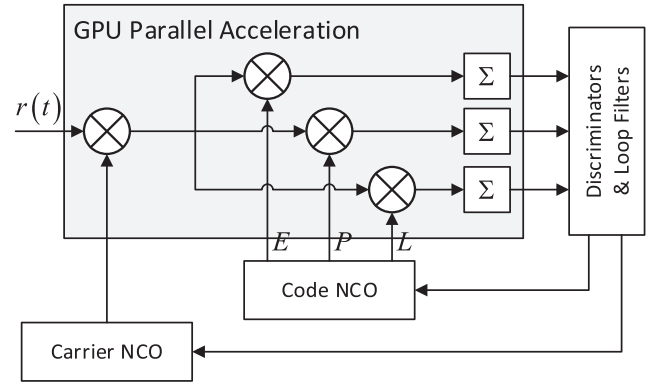

FIGURE 7 Tracking architecture of the real-time software receiver for conventional Binary Phase-Shift Keying (BPSK) signals

accumulate. The code optimizations can be done by having access to the shared memory instead of global memory access and loop unrolling. The grid we chose in CUDA is a one-dimensional structure, and the size of the grid in blocks is equal to the number of tracking channels. The thread blocks we chose in CUDA are also one-dimensional structures with the size of 256 threads. Since the multiplication of two signals is very suitable for vectorization, it is easy to implement the parallel multiplication in CUDA. In addition, since the accumulation of correlation results can be treated as a common tree-based reduction problem, the accumulation operation could be easily optimized via parallel reduction based on the sequential addressing and loop unrolling in CUDA.[21]

5.2 | Unambiguous tracking method for QMBOC signal

Compared with the conventional BPSK signal, the BOC modulated signal has a better spectral separation and wider root mean square (RMS) bandwidth, which means larger advantages on ranging accuracy. However, the BOC modulated signal also introduces a well-known ambiguity threat into the code tracking process because of its sawtooth-like, piecewise linear autocorrelation function (ACF). Therefore, unambiguous tracking methods for BOC signals are of increasing interest. In order to fully exploit the pilot component of the B1C signal, an unambiguous tracking method based on multidimensional loops estimation is proposed to solve the ambiguity problem of QMBOC. It can also be used for the matching reception of the pilot component of the B1C signal. The proposed unambiguous tracking method for the QMBOC signal uses two dual estimators[26,27] to track the narrowband BOC(1,1) component and the wideband BOC(6,1) component in phase quadrature, respectively.

Figure 8 shows the coherent early-late processing (CELP) implementation of the multidimensional loops estimation technique for QMBOC signal unambiguous tracking. The noncoherent early-late processing (NELP) implementation can be similarly obtained. Therefore, it is not difficult to derive the coherent integration results of the in-phase and quadrature-phase components, which can be expressed as follows:

$$
\begin{cases}
I_{1EP} \approx \sqrt{\gamma} R_{BPSK(1)}(\Delta\tau - \Delta_c/2) \\
I_{1LP} \approx \sqrt{\gamma} R_{BPSK(1)}(\Delta\tau + \Delta_c/2) \\
I_{1PE} \approx \sqrt{\gamma} \mathrm{trc}_1(\Delta\tau - \Delta_{s1}/2) \\
I_{1PL} \approx \sqrt{\gamma} \mathrm{trc}_1(\Delta\tau + \Delta_{s1}/2) \\
I_{1PP} \approx \sqrt{\gamma} R_{BOC(1,1)}(\Delta\tau)\cos(\Delta\varphi) \\
I_{2PP} \approx -\sqrt{1-\gamma} R_{BOC(6,1)}(\Delta\tau)\sin(\Delta\varphi)
\end{cases}
, \quad (12)
$$

$$
\begin{cases}
Q_{2EP} \approx \sqrt{1-\gamma} R_{BPSK(1)}(\Delta\tau - \Delta_c/2) \\
Q_{2LP} \approx \sqrt{1-\gamma} R_{BPSK(1)}(\Delta\tau + \Delta_c/2) \\
Q_{2PE} \approx \sqrt{1-\gamma} \mathrm{trc}_2(\Delta\tau - \Delta_{s2}/2) \\
Q_{2PL} \approx \sqrt{1-\gamma} \mathrm{trc}_2(\Delta\tau + \Delta_{s2}/2) \\
Q_{2PP} \approx \sqrt{1-\gamma} R_{BOC(6,1)}(\Delta\tau)\cos(\Delta\varphi) \\
Q_{1PP} \approx -\sqrt{\gamma} R_{BOC(1,1)}(\Delta\tau)\sin(\Delta\varphi)
\end{cases}
, \quad (13)
$$

where $\gamma = 29/33$ is the power ratio of the narrowband BOC(1,1) component to the whole QMBOC component; $R_{BPSK(1)}$ is the correlation function in the code dimension with a triangle shape; trc_1 and trc_2 are the periodic sawtooth-like correlation functions of the narrowband BOC(1,1) component and the wideband BOC(6,1) component, respectively; $R_{BOC(1,\ 1)}$ and $R_{BOC(6,\ 1)}$ are the multipeak correlation functions of the narrowband BOC(1,1) component and the wideband BOC(6,1) component, respectively; Δ_{s1} and Δ_{s2} are the discriminator spacing of subcarrier 1 from the narrowband BOC(1,1) component and subcarrier 2 from the wideband BOC(6,1) component, respectively; and $\Delta\varphi$ is the estimation error of carrier phase.

The output results of the correlators with the prompt replica in both code and subcarrier dimensions can be merged by the following rules:

$$
\begin{cases}
I' = \sqrt{\gamma} I_{1PP} + \sqrt{1-\gamma} Q_{2PP} = R_{QMBOC}(\Delta\tau)\cos(\Delta\varphi) \\
Q' = -\sqrt{\gamma} Q_{1PP} - \sqrt{1-\gamma} I_{2PP} = R_{QMBOC}(\Delta\tau)\sin(\Delta\varphi)
\end{cases}
, \quad (14)
$$

where R_{QMBOC} is the correlation function of the QMBOC modulated signal. Therefore, the conventional Phase Locked Loop (PLL) discriminators can be directly
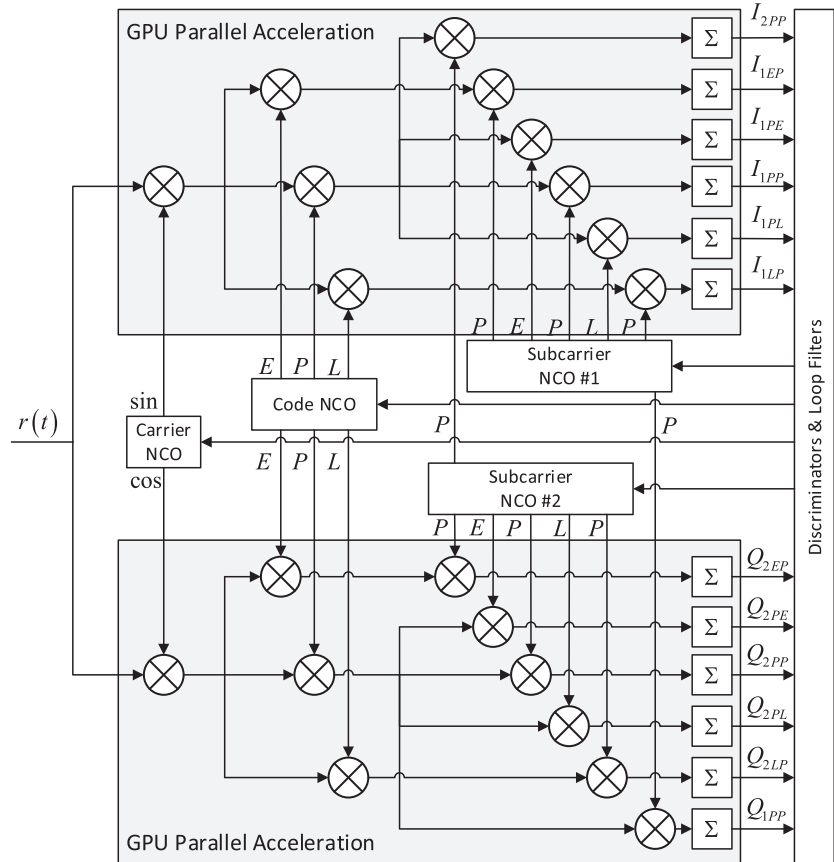

FIGURE 8 Coherent early-late processing (CELP) implementation of multidimensional loops estimation technique

employed to obtain the estimation error of carrier phase, $\Delta\varphi$.

The output results of the correlators with early and late replicas in the code dimension can be merged by the following rules:

$$\begin{cases} E_c = \sqrt{\gamma}I_{1EP} + \sqrt{1-\gamma}Q_{2EP} = R_{BPSK(1)}(\Delta\tau - \Delta_c/2) \\ L_c = \sqrt{\gamma}I_{1LP} + \sqrt{1-\gamma}Q_{2LP} = R_{BPSK(1)}(\Delta\tau + \Delta_c/2) \end{cases}.$$
(15)

Therefore, the conventional Delay Locked Loop (DLL) discriminators can be directly employed to obtain the estimation error of the code delay, $\Delta\tau$.

The output results of the correlators with early and late replicas in the subcarrier dimension from BOC(1,1) and BOC(6,1) components, respectively, can be denoted as follows:

$$\begin{cases} I_{1PE} \approx \sqrt{\gamma}\mathrm{trc}_1(\Delta\tau - \Delta_{s1}/2) \\ I_{1PL} \approx \sqrt{\gamma}\mathrm{trc}_1(\Delta\tau + \Delta_{s1}/2) \end{cases},$$
(16)

$$\begin{cases} Q_{2PE} \approx \sqrt{1-\gamma}\mathrm{trc}_2(\Delta\tau - \Delta_{s2}/2) \\ Q_{2PL} \approx \sqrt{1-\gamma}\mathrm{trc}_2(\Delta\tau + \Delta_{s2}/2) \end{cases}.$$
(17)

These output results have similar characteristics to the correlator outputs for the conventional BPSK signal tracking when ignoring the periodicity. Therefore, similar DLL discriminators can be employed in these two Subcarrier Locked Loops (SLL) to obtain the estimation errors of the subcarrier delay, $\Delta\tau_1$ and $\Delta\tau_2$.

After discriminators and loop filters, a lower accuracy but unambiguous estimate of the delay in code dimension, $\hat{\tau}_c$, from DLL can be obtained, and two higher accuracy but ambiguous estimates of the delay in subcarrier dimensions, $\hat{\tau}_{s1}$ and $\hat{\tau}_{s2}$, from SLLs can also be acquired. Since the delay in code dimension of the received signal is strictly equal to that in subcarrier dimension, unambiguous $\hat{\tau}_c$ can be used to correct $\hat{\tau}_{s1}$ and $\hat{\tau}_{s2}$, respectively, to get two unambiguous and high-precision estimates of the delay, which can be expressed as follows:

$$\begin{cases} \hat{\tau}_1 = \hat{\tau}_{s1} + \mathrm{round}\left(\dfrac{\hat{\tau}_c - \hat{\tau}_{s1}}{T_{s1}}\right) \times T_{s1} \\ \hat{\tau}_2 = \hat{\tau}_{s2} + \mathrm{round}\left(\dfrac{\hat{\tau}_c - \hat{\tau}_{s2}}{T_{s2}}\right) \times T_{s2}, \end{cases}$$
(18)

where $T_{s1} = 1/2f_{sc1}$ and $T_{s2} = 1/2f_{sc2}$ are the chip period of subcarrier 1 and subcarrier 2, respectively. Finally, a single estimate of the delay can be produced using a weighted linear combination of these two corrected estimates that can be expressed as follows:

$$\hat{\tau} = w_1\hat{\tau}_1 + (1 - w_1)\hat{\tau}_2,$$
(19)

where $0 < w_1 \leq 1$ is the normalized weight of $\hat{\tau}_1$. It should be noted that w_1 does not need to be a constant throughout the tracking phase. Since the power of the narrow-band BOC(1,1) component accounts for 29/33 of the entire QMBOC signal, it should be assigned a large w_1 during initial tracking and low carrier-to-noise ratio (C/N_0) conditions. The recommended w_1 under these conditions is in the range of $0.95 \leq w_1 \leq 1$ to make sure the received signal can be continuously tracked. As C/N_0 increases, and the receiver reaches steady-state tracking, w_1 can gradually decrease to strive for the performance improvement brought by the wideband BOC(6,1) component. The recommended w_1 during steady-state tracking is in the range $0.8 \leq w_1 \leq 0.95$ to keep a good balance between accuracy and stability. In addition, the optimal discriminator spacing selection rule of the multidimensional loops estimation technique can also be used to strive for better tracking performance.[28]

6 | EXPERIMENTAL RESULTS

Table 3 shows the configuration of our real-time software receiver for civil BDS-3 signals. The full L-band antenna with LNA we chose is the HX-GSX81A from Harxon Corporation, and it was laid on the roof of the Weiqing Building of Tsinghua University in Beijing during the whole test. The down-converter is the BDC-L-210-4C made by HeBei Doheart Electronic Technology Co, LTD. The data acquisition card is an X5-210 M developed by Innovative Integration. The main program of the software receiver runs on an ordinary PC, which is equipped with an Intel i7-4790 K CPU, an NVidia GeForce GTX 970 GPU, and a CUDA parallel programming platform whose version number is 8.0.

TABLE 3 Configuration of BeiDou Navigation Satellite System (BDS-3) real-time software receiver

No.	Equipment/Environment	Model/Version Number
1	Full L-band Antenna	Harxon Corporation HX-GSX81A
2	Down converter	HeBei Doheart Electronic Technology Co.,LTD. BDC-L-210-4C
3	Data acquisition card	Innovative Integration X5-210 M
4	CPU	Intel i7-4790 K
5	GPU	NVidia GeForce GTX 970
6	CUDA	8.0

According to the launch list of BDS satellites published by the China Satellite Navigation Office (CSNO), 16 BDS-3 MEO satellites have been placed on orbit as of 18 October 2018 and their pseudorandom noise (PRN) sequence numbers are 20, 47, 27, 48, 21, 22, 29, 30, 23, 24, 25, 26, 32, 33, 34, and 35, respectively.

Since the operating statuses of the existing BDS-3 satellites are all in test, positioning test results cannot be provided right now. The following experiments include four aspects, namely, real-time tracking of BDS-3 signals, C/N_0 monitoring, signal processing monitoring, and the verification and analysis of the proposed algorithms. It should be noted that all the experiments are carried out using the actual signals broadcast by the BDS satellites.

Figure 9 shows the real-time tracking of civil BDS-3 signals in four frequencies at Tsinghua University on 22 July 2018. It can be seen that all the civil BDS-3 signals, which include B2a, B3I, B1I, and B1C signals, could be successfully received and processed. The Doppler frequency of the received signal is indeed proportional to the carrier center frequency. In addition, there are two modes we used in the tracking of the pilot component of the B1C signal: the matching reception of the QMBOC signal which is referred to as B1CM, and the mismatched tracking called B1C, which ignores the wideband BOC(6,1) component. It can be seen from Figure 9 that the C/N_0 in the matching reception mode is around 0.4 dB higher than that in mismatched tracking mode. Since the power of the wideband BOC(6,1) component accounts for 4/33 of the entire QMBOC signal, the BOC(6,1) component could provide the matching

reception mode with the energy gain of about 0.5 dB in theory, which is close to our observation. Therefore, these results verify the correctness and effectiveness of the proposed unambiguous tracking method of the QMBOC signal.

Figure 10 shows the B1I (PRN 20) in-phase correlation results between the prompt replica signal and the received baseband signal during steady-state tracking. It can be seen from Figure 10 that the navigation bits can be successfully demodulated, thus verifying the correctness of the proposed architecture of the real-time software receiver.

Figure 11 shows the C/N_0 monitoring results of BDS-3 signals at Tsinghua University for 24 hours from 25 July 2018. It can be seen from Figure 11 that the visible time of MEO satellites at Beijing is around 7 hours. In addition, the time during which four satellites can be seen simultaneously is between 2 and 3 hours.

Figure 12 shows the monitoring results of the real-time correlation peak shape for B2a and B1C pilot components. The B2a pilot component adopts BPSK(10) modulation, and its ACF has one main peak. Since the sampling rate of B2a is 20 MHz, which is just enough to contain the main lobe of the B2a signal, the peak of its ACF is relatively smooth because of the influence of band-limited filtering. The B1C pilot component adopts QMBOC(6,1,4/33) modulation, and its ACF has two side peaks. Since the sampling rate of B1C we chose is 20 MHz, which is wide enough relative to the main lobe of the B1C signal, the peak of its ACF is very sharp.

```
CHid    PRN    Status  Lock    C/N0    Doppler         TransmitTime
--------------------------------------------------------------------------
Succeed to initialize CUDA device.
*****************************************BDS B1*********************************************
1       20     CCDF    0.99    50.39   920.53462720    44245.24969457
2       29     CCBF    0.98    47.20   -356.69385945   44245.24616416
3       30     CCBF    0.97    45.06   -2885.58991464  44245.24451439

*****************************************BDS B3*********************************************
1       20     CCBF    1.00    54.41   754.37372028    44245.24969462
2       29     CCBF    0.99    51.09   -289.93103962   44245.24616420
3       30     CCBF    0.99    48.93   -2344.92836709  44245.24451442

*****************************************BDS B1C********************************************
1       20     CCBF    0.99    50.70   937.01893764    44245.24969460
2       29     CCBF    0.98    47.61   -359.95868342   44245.24616420
3       30     CCBF    0.97    45.30   -2911.97098941  44245.24451442

*****************************************BDS B1CM*******************************************
1       20     CCBF    0.99    51.07   937.03017137    44245.24969460
2       29     CCBF    0.98    48.04   -359.94108343   44245.24616420
3       30     CCBF    0.97    45.76   -2911.97348760  44245.24451442

*****************************************BDS B2a********************************************
1       20     CCBF    0.99    52.17   699.75381293    44245.24969458
2       29     CCBF    0.99    48.51   -268.75503375   44245.24616417
3       30     CCBF    0.97    45.21   -2174.59248715  44245.24451439
```

FIGURE 9 Screenshot of tracking civil BeiDou Navigation Satellite System (BDS-3) signals in four frequencies at Tsinghua University on 22 July 2018
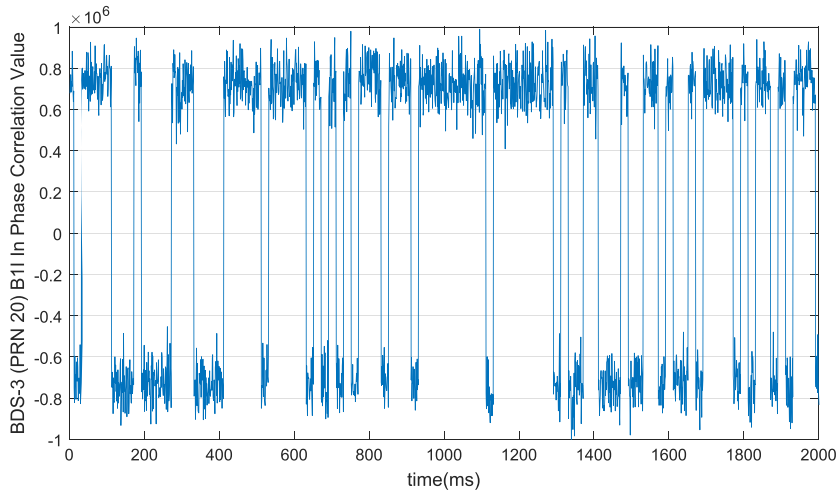
FIGURE 10 BeiDou Navigation Satellite System (BDS-3) (PRN 20) B1I in phase correlation results [Color figure can be viewed at wileyonlinelibrary.com and www.ion.org]
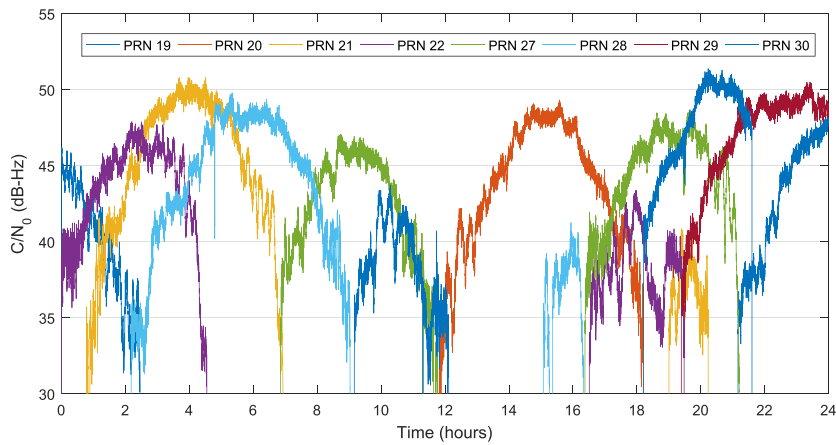

FIGURE 11 Monitoring results of BeiDou Navigation Satellite System (BDS-3) signals at Tsinghua University from 25 July 2018 to 26 July 2018 [Color figure can be viewed at wileyonlinelibrary.com and www.ion.org]
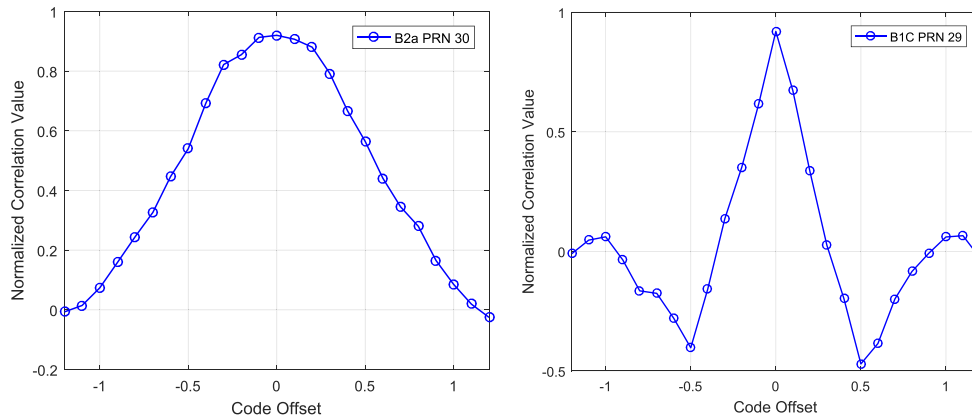

FIGURE 12 Monitoring results of real-time correlation peak shape [Color figure can be viewed at wileyonlinelibrary.com and www.ion.org]

Table 4 shows the comparison results of the required time between the traditional direct acquisition and the proposed B1I aided acquisition. Since the B3I signal has the same modulation with the pilot component of the B2a signal, the acquisition time required for these two signals is very close. Therefore, the comparison of the acquisition time mainly includes three civil signals, which are the B1I, B2a, and B1C signals. Comparing the rows in Table 4, the following results can be seen. First, the time required for parallel acquisition of multiple

TABLE 4 Comparison of the required time between the direct acquisition and the B1I-aided acquisition

| Signals | Parameters | | | | | Acquisition Time | |
	Sampling Rate	Coherent	Frequency Bin	Noncoherent	Channels	Direct Acquisition	B1I-Aided Acquisition
B1I	5 MHz	1 ms	500 Hz	1	1	0.3535 ms	--
	5 MHz	1 ms	500 Hz	10	1	1.4479 ms	--
	5 MHz	1 ms	500 Hz	1	12	0.5715 ms	--
	5 MHz	1 ms	500 Hz	10	12	2.5601 ms	--
B2a/B3I	20 MHz	1 ms	500 Hz	1	1	0.7055 ms	0.0821 ms
	20 MHz	1 ms	500 Hz	10	1	4.9834 ms	0.4826 ms
	20 MHz	1 ms	500 Hz	1	12	1.3065 ms	0.0943 ms
	20 MHz	1 ms	500 Hz	10	12	9.4649 ms	0.5134 ms
B1C	20 MHz	10 ms	50 Hz	1	1	48.7478 ms	0.5096 ms
	20 MHz	10 ms	50 Hz	10	1	69.0209 ms	2.7568 ms
	20 MHz	10 ms	50 Hz	1	12	50.3513 ms	Not enough satellites
	20 MHz	10 ms	50 Hz	10	12	71.4458 ms	Not enough satellites

TABLE 5 Tracking time required for the Compute Unified Device Archite (CUDA)-based correlators

| Signals | Parameters | | | | Tracking Time |
	Sampling Rate	Channels	Coherent	Noncoherent	
B1I	5 MHz	1	1 ms	1	0.0714 ms
	5 MHz	12	1 ms	1	0.0732 ms
B2a/B3I	20 MHz	1	1 ms	1	0.0930 ms
	20 MHz	12	1 ms	1	0.0969 ms
B1C	20 MHz	1	10 ms	1	0.1393 ms
	20 MHz	12	10 ms	1	Not enough satellites

channels is positively related to the sampling rate, the coherent integration time, the number of channels, and the times of the noncoherent accumulations. Second, compared with the traditional direct acquisition, the B1I-aided acquisition method can greatly reduce the required time. Third, for fixed sampling rate and coherent integration time, the times of noncoherent accumulations have a greater influence on the required acquisition time than the number of channels. Fourth, when the channel numbers and the times of noncoherent accumulations are fixed, the increase of the coherent integration time will significantly increase the required acquisition time. This is because long-coherent integration time means a large amount of data required to process.

Table 5 shows the tracking time required for the CUDA-based correlators at three frequencies in a quantitative way. Since the B3I signal has the same modulation with the pilot component of the B2a signal, meaning that the computational performance of these two signals in the tracking phase is similar, the tracking time of the B2a signal can be predicted by that of the B3I signal. It can be seen from Table 5 that the tracking time of the CUDA-based correlators is very short, which means up to hundreds of correlators can work simultaneously in

real-time mode. In addition, it can also be seen that the number of channels has a very limited influence on the required tracking time, which means the CUDA-based correlators are more cost-effective for tracking multiple channels as opposed to only one channel.

7 | CONCLUSIONS AND FUTURE WORK

We have designed and implemented a GPU-based real-time software receiver capable of processing all civil BDS-3 signals in parallel. In addition, a complete description of all signal processing aspects including front-end processing and baseband signal processing is given. The work and contribution of our discussion mainly include three aspects.

First, a GPU-based real-time software receiver architecture is designed and implemented, which can process all civil BDS-3 signals in parallel. It could be used in signal performance analysis, signal quality monitoring, and processing algorithm development. Moreover, a complete description of all signal processing aspects including front-end processing and baseband signal processing is

given. The actual tests verify the correctness of the proposed architecture. Therefore, it could provide guidance to receiver designers who need to analyze and process civil BDS-3 signals.

Second, a B1I-aided acquisition method is applied to reduce the search space of other BDS-3 signals from the same satellite. Compared with the traditional acquisition methods, the B1I-aided acquisition method utilizes the highly correlated characteristics between the B1I signal and other signals from the same satellite to achieve faster acquisition and to reduce the reliance on high-performance hardware. The test results from actual signals show that the B1I-aided acquisition method is correct and effective. Therefore, the applied B1I-aided acquisition method can provide the reference value for the acquisition of multiple signals at different frequencies in other GNSSs.

Third, an unambiguous tracking method based on multidimensional loops estimation is proposed to solve the ambiguity problem of the QMBOC signal, which can be used for the matching reception of the pilot component of the B1C signal. The actual test results verify the correctness of the method. In addition, the recommended weight selection range is given during initial tracking and steady-state tracking phase, which is useful for receiver designers and users.

For future research, the joint processing of multiple BDS-3 signals is recommended. In addition, the optimal parameter selection rule for unambiguous tracking of the QMBOC signal based on multidimensional loops estimation technique is also recommended.

ACKNOWLEDGEMENT

ORCID

Yang Gao https://orcid.org/0000-0002-2177-5804
Zheng Yao https://orcid.org/0000-0002-7657-644X

REFERENCES

1. China Satellite Navigation Office. Launch lists of BDS satellites. http://www.beidou.gov.cn/xt/fsgl/, accessed on December 9, 2018.

2. Yang Y, Xu Y, Li J, Yang C. Progress and performance evaluation of BeiDou global navigation satellite system: Data analysis based on BDS-3 demonstration system. *Sci China Earth Sci.* May 2018;61(5):614-624.

3. Yang Y, Li J, Xu J, Tang J, Guo H, He H. Contribution of the compass satellite navigation system to global PNT users. *Chin Sci Bull.* September 2011;56(26):2813-2819.

4. China Satellite Navigation Office. BeiDou navigation satellite system signal in space interface control document open service signal (Version 2.1); November 2016.

5. China Satellite Navigation Office. BeiDou savigation satellite system signal in space interface control document open service signal B1C (Version 1.0); December 2017.

6. China Satellite Navigation Office. BeiDou navigation satellite system signal in space interface control document open service signal B2a (Version 1.0); December 2017.

7. China Satellite Navigation Office, BeiDou navigation satellite system signal in space interface control document open service signal B3I (Version 1.0); February 2018.

8. Borre K, Akos DM, Bertelsen N, Rinder P, Jensen SH. *A Software-defined GPS and Galileo receiver: a single-frequency approach.* Boston: Springer Science & Business Media; 2007.

9. Hobiger T, Gotoh T, Amagai J, Koyama Y, Kondo T. A GPU-based real-time GPS software receiver. *GPS Sol.* March 2010;14(2):207-216.

10. Huang B, Yao Z, Guo F, Deng S, Cui X, Lu M. *STARx—A GPU Based Multi-System Full-Band Real-Time GNSS Software Receiver. Proceedings of the 26th International Technical Meeting of the Satellite Division of The Institute of Navigation (ION GNSS+ 2013).* Nashville, TN; September 2013:1549-1559.

11. Park KW, Yang JS, Park C, Lee MJ. *Implementation of GPGPU Based Real-Time Signal Acquisition and Tacking Module for Multi-Constellation GNSS Software Receiver.* Proceedings of the 27th International Technical Meeting of the Satellite Division of The Institute of Navigation (ION GNSS+ *2014*). Tampa, FL; September 2014:1410-1416.

12. Yao Z, Zhang J, Lu M. ACE-BOC: Dual-frequency constant envelope multiplexing for satellite navigation. *IEEE Trans Aero Electron Syst.* April 2016;52:466-485.

13. Hein GW, Avila-Rodriguez JA, Wallner S, et al. *MBOC: The New Optimized Spreading Modulation Recommended for GALILEO L1 OS and GPS L1C. Proceedings of IEEE/ION PLANS 2006.* San Diego, CA; April 2006:883-892.

14. Yao Z, Lu M, Feng Z. Quadrature multiplexed BOC modulation for interoperable GNSS signals. *Electron Lett.* August 2010;46:1234-1236.

15. Yao Z, Lu M. *Optimized Modulation for Compass B1-C Signal with Multiple Processing Modes.* Proceedings of the 24th International Technical Meeting of the Satellite Division of The Institute of Navigation (ION GNSS 2011). Portland, OR; September 2011:1234-1242.

16. Takasu T. RTKLIB: An open source program package for GNSS positioning. http://www.rtklib.com, accessed on July 2, 2018.

17. Bertelsen PRN. *Design of a Single Frequency GPS Software Receiver.* Master's Thesis. Aalborg: Aalborg University; 2004.

18. Krumvieda K, et al. A complete IF software GPS receiver: A tutorial about the details. Proceedings of the 14th International Technical Meeting of the Satellite Division of The Institute of Navigation (ION GPS 2001); Salt Lake City, UT, September 2001:789–829.

19. Cheng U, Hurd WJ, Statman JI. Spread-spectrum code acquisition in the presence of Doppler shift and data modulation. *IEEE Trans Comm.* February 1990;38:241-250.

20. Van Nee DJR, Coenen A. New fast GPS code-acquisition technique using FFT. *ElectronLett.* January 1991;27:158-160.

21. Mark H. Optimizing parallel reduction in CUDA. *NVIDIA CUDA SDK*, 2008.

22. Lim DW, Moon SW, Park C, Lee SJ. L1/L2CS GPS Receiver Implementation with Fast Acquisition Scheme. *Proceedings of IEEE/ION PLANS 2006.* San Diego, CA; April 2006:840-844.

23. Macchi-Gernot F, Petovello MG, Lachapelle G. Combined acquisition and tracking methods for GPS L1 C/A and L1C signals. *Int J Navi Observ.* 2010;2010:1-19.

24. Yuan H, Lv J, Yu Y, Chang J. A Fast Acquisition Algorithm for L1C Based on L1CA and L1C Combined Detection. *Proceedings of the 2012 China Satellite Navigation Conference (CSNC).* Berlin, Heidelberg: Springer; May 2012:689-698.

25. Kaplan E, Hegarty C. *Understanding GPS: Principles and applications.* Norwood, MA: Artech House; 2005.

26. Hodgart MS, Blunt PD, Unwin M. The Optimal Dual Estimate Solution for Robust Tracking of Binary Offset Carrier (BOC) Modulation. *Proceedings of the 20th International Technical Meeting of the Satellite Division of The Institute of Navigation (ION GNSS 2007).* Fort Worth, TX; September 2007:1017-1027.

27. Borio D. Double phase Estimator: new unambiguous binary offset carrier tracking algorithm. *IET Radar, Sonar Navi.* August 2014;8:729-741.

28. Gao Y, Yao Z, Lu M. Theoretical analysis of unambiguous 2-D tracking loop performance for band-limited BOC signals. *GPS Sol.* January 2018;22:1-13.